ELSEVIER

Contents lists available at ScienceDirect

# Journal of Power Sources

journal homepage: www.elsevier.com/locate/jpowsour



# Reconfigurable solid-state electrolytes for high performance flexible supercapacitor



Sanghyun Hong<sup>a,1</sup>, Hyehee Kim<sup>a,1</sup>, Sen Gao<sup>a</sup>, Rodrigo L. Lavall<sup>a,b,\*\*\*</sup>, Hyun Young Jung<sup>c,\*\*</sup>, Yung Joon Jung<sup>a,\*</sup>

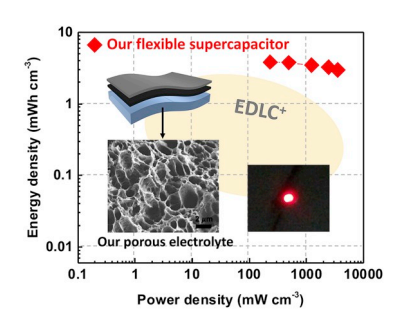
- <sup>a</sup> Department of Mechanical and Industrial Engineering, Northeastern University, Boston, MA, 02115, USA
- b Department of Chemistry, Federal University of Minas Gerais. Av. Antônio Carlos, 6627 Pampulha, CEP 31270-901, Belo Horizonte, MG, Brazil
- <sup>c</sup> Department of Energy Engineering, Gyeongnam National University of Science and Technology, Jinju, Gyeongnam, 52725, South Korea

#### HIGHLIGHTS

#### Reconfigurable/solvent exchangeable electrolytes with highly controlled nanopores.

- Highly integrated structure that results in increase ion accessibility/mobility.
- Ionic liquid based solid-state supercapacitor exhibits stable operation at 2 V
- High power and energy density, and excellent long-term stability with 10 K cycles.

#### GRAPHICAL ABSTRACT



#### ARTICLE INFO

Keywords: Flexible supercapacitor Reconfigurable electrolyte Nanoporous film Carbon nanotubes

#### ABSTRACT

To realize high performance and a flexible supercapacitor, it is necessary to address the fundamental issues including low ionic conductivity of solid electrolytes and high interfacial resistance of electrode/electrolyte pairs. Here we present unique solid-state electrolytes by integrating highly engineered nano-porous polyvinyl alcohol (PVA) with super-flat vertically aligned single-walled carbon nanotubes (VA-SWNTs). Highly engineered PVA nano-porous films are fabricated by a generic freeze-thaw process followed by water-miscible solvent treatment in order to create highly controlled nano/microscale pores inside of PVA. Such highly porous PVA films act as both reconfigurable electrolyte template and separator where H<sub>3</sub>PO<sub>4</sub> aqueous solution or ionic liquids can be selectively inserted for a variety of power requirements in flexible electronic applications. Our developed pore formation process is suitable for directly integrating high performance VA-SWNTs electrode as it allows the effective permeation of the polymer electrolyte into nanoscale inter-tube space enabling the easy access and faster transport of ions for higher power capability. This unique entity of reconfigurable electrolyte and nanostructured electrode demonstrates high power and energy densities and remarkable stability after 10,000 charge/discharge cycles.

<sup>\*</sup> Corresponding author. Department of Mechanical and Industrial Engineering, Northeastern University, Boston, MA, 02115, USA.

<sup>\*\*</sup> Corresponding author. Department of Energy Engineering, Gyeongnam National University of Science and Technology, Jinju, Gyeongnam, 52725, South Korea.

\*\*\* Corresponding author. Department of Chemistry, Federal University of Minas Gerais. Av. Antonio Carlos, 6627 Pampulha, CEP 31270-901, Belo Horizonte, MG, Brazil.

 $<sup>\</sup>textit{E-mail addresses:} \ rodrigo. lavall@qui.ufmg.br\ (R.L.\ Lavall),\ hyjung@gntech.ac.kr\ (H.Y.\ Jung),\ jungy@coe.neu.edu\ (Y.J.\ Jung).$ 

 $<sup>^{1}\,</sup>$  Authors equally contributed.

#### 1. Introduction

Flexible supercapacitor devices have attracted great interests for various future electronic systems, including bendable displays, portable electronic papers, and wearable multimedia [1–7]. Particularly solid-state supercapacitors have several important advantages over their liquid electrolyte counterparts such as no concern for any electrolyte leakage, ease of handling, lightweight and small size, improved stability and flexible structural design [8–13]. These flexible solid-state supercapacitor devices have been developed by sandwiching the flexible polymer-based electrolytes between two electrodes [1,14–25]. Among various types of polymeric electrolytes, a hydrogel polymer electrolyte has been extensively used due to its composition of a polymer matrix and aqueous liquid electrolyte [15,26–28]. PVA is one of the most widely used hydrogel polymer electrolytes, as it provides high porosity, high

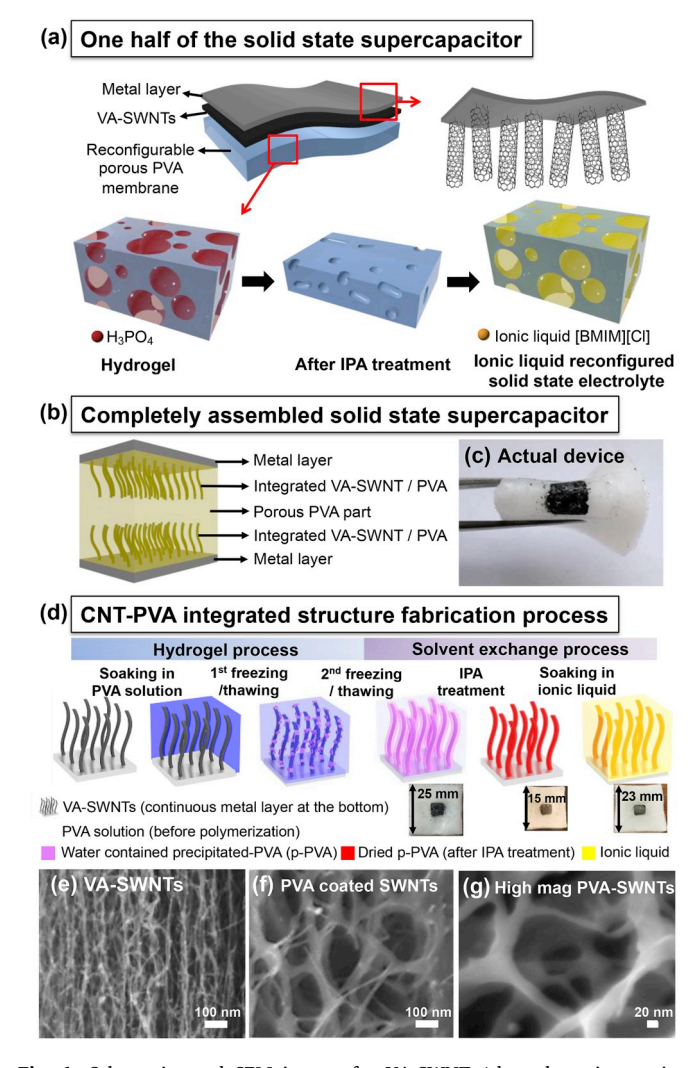


Fig. 1. Schematics and SEM images for VA-SWNTs/electrolytes integration system. (a) The schematic of one half of the solid-state supercapacitor and reconfigurable porous PVA membrane at hydrogel state, solid-state, and ionic liquid contained sol-gel state. (b) A schematic of the completely assembled cell where a metal layer/VA-SWNTs/PVA unit was faced against another PVA/VA-SWNTs/a metal layer unit. (c) Photograph of the actual device. (d) The schematic of sample preparation and the inserts are the actual photographs of VA-SWNTs/electrolyte integrated system at hydrogel state, solid-state (after IPA treatment), and ionic liquid contained sol-gel state respectively. (e) SEM image of highly organized original SWNTs that have a narrow diameter as small as 0.8 nm to several tens of nm with a distance around 10 nm between SWNTs. (f), (g) SEM image after the solvent exchange process (IPA treatment), we have observed PVA coated SWNTs.

ionic conductivity, and great mechanical properties through the freeze-thawing process [29–34]. However, hydrogel polymer electrolytes have limitations on increasing electrochemical window since it is made with an aqueous liquid electrolyte which contains a considerable amount of water, lowering energy density and reliability of supercapacitors [8,12]. Also hydrogel polymer electrolytes have a poor contact at the electrode/electrolyte interface, as polymer electrolytes cannot penetrate into electrodes' pores. This often results in pore collapse and non-conformal electrode/electrolyte interfaces causing high contact resistance and poor electrochemical performance [35]. Especially considering the explosive interest of using highly porous nanocarbon materials and their architectures (ex: high-density VA-SWNTs or stacked graphene) towards high performance multifunctional electrodes, addressing this challenge is immense both from fundamentals and applied perspectives [1,36–47].

Here we present a generic approach to rationally design and build all-solid-state and reconfigurable supercapacitors by integrating PVA based solvent exchangeable membranes and super-flat VA-SWNTs. Highly porous VA-SWNTs films combined with PVA hydrogel was fabricated through the freeze-thawing method to configure the electrode/electrolyte integrated supercapacitor devices [48]. To obtain the completely dried VA-SWNTs/PVA membrane without a pore collapse, the 2-isopropyl alcohol (IPA) exchange process was conducted by performing a stepwise concentration increase of the IPA against water based the hydrogels. Such controllably designed porous PVA film acts like a sponge absorbing a large amount of desired liquid electrolytes (H<sub>3</sub>PO<sub>4</sub> aqueous electrolyte or 1-butyl-3-methylimidazolium chloride (BMIMCl including 15% water)) for higher capacitance. Also, its nano/microscale pores contain liquid electrolytes effectively even under severe mechanical deformation. Our reconfigurable solid-state flexible capacitor devices show better electrochemical properties and excellent cycling stability due to the preserved high surface area of the electrode resulting from the effective permeation of the polymer electrolyte, and the improved electrode/electrolyte interface that enables excellent charge accessibility. The integrated reconfigurable electrode/electrolyte systems also allow the fabrication of very thin, lightweight, flexible all-solid-state, and high-performance supercapacitors for uses in the portable, wearable, flexible electronic and structural energy devices for utilization as part of a wing or fuselage of communications satellites, unmanned aerial vehicles, aircraft, submarines, and others.

#### 2. Experimental

### 2.1. Synthesis of VA-SWNTs electrode

VA-SWNTs were synthesized by thermal chemical vapor deposition (CVD) system. Anhydrous ethanol (Sigma-Aldrich, 99.95%) was for a carbon source, and 3–5 Å thick cobalt (Co) catalyst on 20–30 nm aged aluminum buffer layer was deposited on a silicon wafer which has 100 nm silicon oxide on top. Operation temperature was controlled to 850  $^{\circ}$ C in a gold-mirror furnace. We have obtained about 30  $\mu$ m long VA-SWNTs with the mass of an average 0.3 mg in the area of 16 mm  $^2$  after 30 min CVD.

# 2.2. Fabrication of porous solid electrolyte and integration of electrolyte/electrode

The PVA (Sigma-Aldrich, Mw 89,000-98,000) was dissolved into water under mechanical stirring at  $150\,^{\circ}$ C using the glass jar (Uline). At the resultant solution, it was added  $1.5\,\mathrm{M\,H_3PO_4}$  (Sigma-Aldrich) solution and mechanically stirred at room temperature for 1 day. This completely dissolved PVA/H<sub>3</sub>PO<sub>4</sub> solution can be crystallized by several times of the freezing/unfreezing process [48]. The pore size and porosity were analyzed by the Image J program using SEM images. The 5 different cross-sectional samples were fabricated, and 15–20 SEM images were taken from each sample. The image J program can select the

pores and calculate the size and porosity overall the selected area (Fig. S2). The average pore size of the PVA film was 380 nm with  $\pm 81.8$  nm of standard deviation.

Chromium metal layer was deposited on the VA-SWNTs upper surface using the sputtering system (MRC 8667) to a thickness of 1  $\mu m$ . The Chromium deposited VA-SWNTs were transferred upside down to a carbon tape on the petri-dish to expose the flat bottom surface upward (for more detail information on transfer methods, refer to our previous paper [49]). Then the PVA/H<sub>3</sub>PO<sub>4</sub> solution was impregnated into the inside of the super-flat VA-SWNTs. The VA-SWNT/PVA pair was maintained in a vacuum desiccator for 30 min to assure good wettability and eliminate air bubbles. In order to enhance the porosity of the electrolyte and the compatibility of the electrolyte/electrode, a freeze-thaw process was performed. The freeze-thawing procedure was repeated two times by freezing at  $-20\,^{\circ}\text{C}$  for 24 h freezing and thawing at room temperature for 30 min. As a result, we have successfully obtained the highly integrated and porous VA-SWNT/PVA film.

#### 2.3. IPA treatment for solvent exchange

For solvent exchange, water in the VA-SWNT/PVA hydrogel film was completely replaced with pure IPA by gradually increasing the concentration of IPA starting with the distilled water/IPA (30%, 50%, and 70%), then pure IPA. After that, the film was completely dried in a vacuum chamber for 3 h. This completely dried PVA film can be soaked into any aqueous solution or hydrophilic ionic liquids for solvent exchange.

#### 2.4. Preparation of IL-based solid-state flexible supercapacitors

The highly integrated and porous VA-SWNT/PVA film was soaked into the  $1.5\,\mathrm{M}\,\mathrm{H}_3\mathrm{PO}_4$  aqueous solution or 1-butyl-3-methylimidazolium chloride (BMIMCl including 15% water) hydrophilic ionic liquid in order to fill the pores with an electrolyte solution. The BMIMCl is typically solid at room temperature, and the 95 wt% BMIMCl is almost a slurry state. For optimal performance of our solid-state flexible supercapacitor, we used the 85 wt% BMIMCl, which is in a liquid state and is the optimized concentration for the best swelling into the porous PVA backbone. Fig. 1a shows an identical half of the supercapacitor structure, where the two halves are conjoined with the reconfigurable porous PVA membranes at the intersection. The PVA membrane was soaked with the  $\mathrm{H}_3\mathrm{PO}_4$  or hydrophilic ionic liquid electrolyte. Top-down pressure was applied to combine the two halves. A scheme of the complete cell assembly is presented in Fig. 1b.

### 2.5. Electrochemical characteristics of the integration supercapacitors

Electrochemical properties of the supercapacitors are analyzed using cyclic voltammetry (CV), galvanostatic charge-discharge (CD), impedance spectroscopy (EIS) and cyclic stability. The CV curves of the devices are measured between 0 and 0.8 V for the H<sub>3</sub>PO<sub>4</sub> aqueous electrolyte and 0-2 V for the ionic liquid electrolyte with various scan rates in a range of  $10-500\,\mathrm{mV\,s^{-1}}$ . The electrochemical impedance spectroscopy measurements were performed over a frequency range from 1 MHz to 0.01 Hz at the amplitude of the sinusoidal voltage of 10 mV on the devices [1,50]. An alternative approach to the impedance analysis is to directly consider the supercapacitor as a whole by using the impedance data. The impedance  $Z(\omega)$  can be written under its complex form  $Z(\omega) = Z'(\omega) + jZ''(\omega)$ , where Z' and Z'' are the real part and the imaginary part of the impedance, respectively, defined as  $|Z(\omega)|^2 = Z^2 + Z^2$ . The capacitance  $C(\omega)$  is defined as  $C(\omega) = C(\omega) + C(\omega)$  $jC''(\omega)$  leading to  $C'(\omega) = -Z''(\omega) / (\omega |Z(\omega)|^2)$ ,  $C''(\omega) = -Z'(\omega) / (\omega |Z(\omega)|^2)$  $(\omega |Z(\omega)|^2)$ , where  $C(\omega)$  and  $C''(\omega)$  are the real part and the imaginary part of the capacitance  $C(\omega)$ . The time constant defined as  $\tau_0 = 1/f_0$ , which is known as a dielectric relaxation time characteristic of the

whole system, is obtained from the maximum  $C''(\omega)$  at frequency  $f_0$ . The CD measurements were carried out at the different current density from 0.1 to  $20\,\mathrm{A\,g^{-1}}$  (considering the mass of the active material, VA-SWNT, in one electrode). Capacitance values where obtained from the galvanostatic charge/discharge experiments (discharge curve) using  $C_{spec.elec} = (2i\Delta t) / (\nu \Delta V)$ , where i is the applied current,  $\Delta t$  is the discharge time,  $\Delta V$  is the discharge voltage after the ohmic drop and  $\nu$ is the volume of the active material (VA-SWNT) in one electrode. The capacitance retention is obtained by performing charge-discharge of the supercapacitor over 10,000 cycles. The power density (P) and energy density (E) of the supercapacitors are calculated from the galvanostatic charge/discharge experiments (discharge curve) using  $E = i \int V dt$  and  $P = E/\Delta t$  (normalized by the total mass (or volume) of the active material (VA-SWNT) in both electrodes), where i is the applied current, V is the discharge voltage after the ohmic drop and  $\Delta t$ is the discharge time.

#### 3. Results and discussion

#### 3.1. Fabrication of the electrode/electrolyte integration system

Fig. 1a is the schematics showing our strategy for fabricating a reconfigurable electrolyte system where super-flat VA-SWNTs are integrated for electrodes. First, PVA was dissolved in water and phosphoric acid solution and evenly poured on VA-SWNT films grown by chemical vapor deposition (CVD) [49,51-53] as shown in Fig. 1e. In order to achieve the maximum number of electrical contacts and stable interfaces between VA-SWNTs and a current collector, we employed a super-flat VA-SWNT film fabricated by multi-step transfer processes, converting super-flat bottom of VA-SWNTs, grown on atomically flat silicon wafer substrates, into the top surface of the electrode (see the methods section) [49]. Then the freeze-thaw method was performed to create PVA hydrogel films (Fig. 1d and Fig. S1). During repetitive cycles of 24 h freezing at -20 °C and 30 min thawing at room temperature, water freezes while expelling PVA and forming the regions of high concentration of PVA. As the PVA chains come into close contact with each other, PVA crystallites form and hydrogen bonding occur [48]. These interactions remain intact even after thawing at room temperature and develop a non-degradable three-dimensional hydrogel network through the continuous freeze-thaw processes [29-34]. The pore size of PVA film is 380 nm with  $\pm 81.8\,\text{nm}$  of standard deviation (analyzed by the Image J program), and its porosity is about  $35 \pm 5\%$ (Fig. S2).

In order to create a reconfigurable electrolyte membrane template, water solvent in the hydrogel film was exchanged by 2-Iso Propyl Alcohol (IPA) by gradually increasing IPA concentration to 100%. The membrane film dried in the air resulted in internal pore collapse (supplement Fig. S3f), while dried by the ion exchange method maintained high porosity inside of the membrane (Fig. 1f and g, and supplement Fig. S3g). We also observed the effective conformal coating of PVA on VA-SWNTs providing highly defined nanoscale pore structures where the high accessibility of ions and electrons could be occurred during the charge and discharge processes. Finally, reconfigurable supercapacitor films were demonstrated by inserting aqueous electrolytes (H<sub>3</sub>PO<sub>4</sub>) or 1-butyl-3-methylimidazolium chloride (BMIMCl including 15% water) ionic liquid electrolytes into a reconfigurable PVA membrane film. The solid-state electrolyte films used in our integrated flexible supercapacitors act as both the electrolyte and separator to avoid short circuit and chemical leakage (Fig. 1c). A scheme of the complete cell assembly where a chromium layer/aligned SWNT/ GEP film unit was faced against another GPE film/aligned SWNT/ chromium unit is presented in Fig. 1b. The complete cell was then placed in a stainless steel coin cell for the electrochemical characterization of the device.

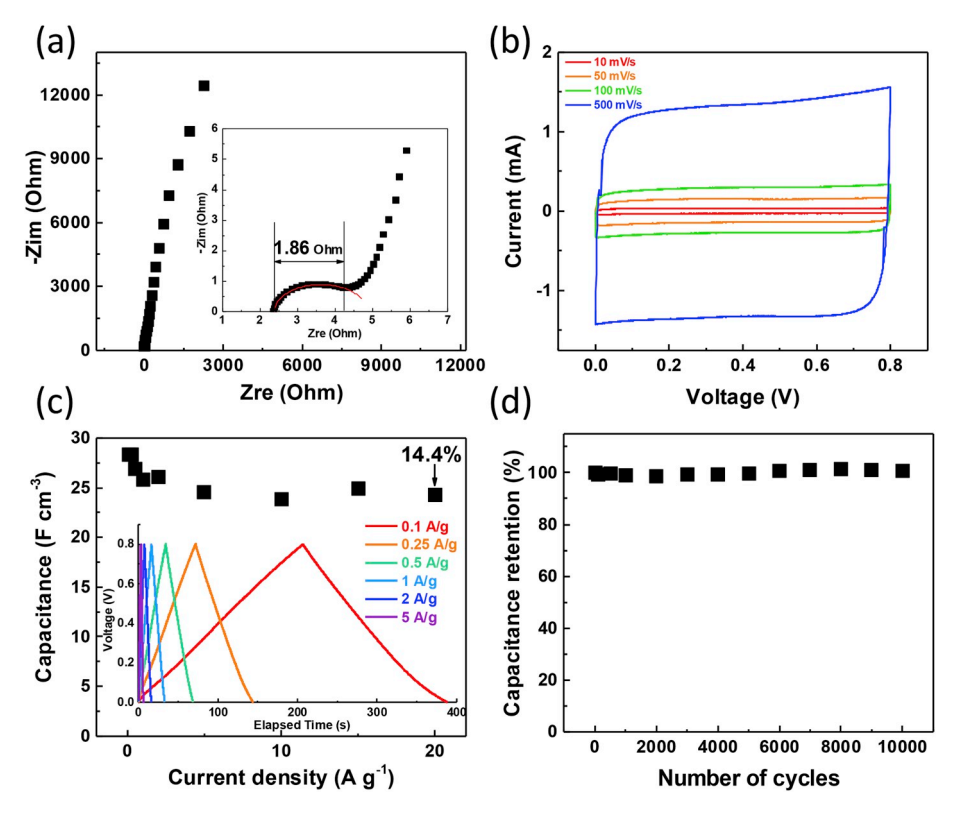


Fig. 2. Electrochemical properties of solid-state supercapacitors with PVA and  $H_3PO_4$  solution. (a) Nyquist impedance plot. (b) Cyclic voltammetry curves at 10, 50, 100, and 500 mV s<sup>-1</sup>. (c) Specific capacitances at various current densities. Inset is Galvano static charge/discharge curves at different current density. (d) Cyclic stability.

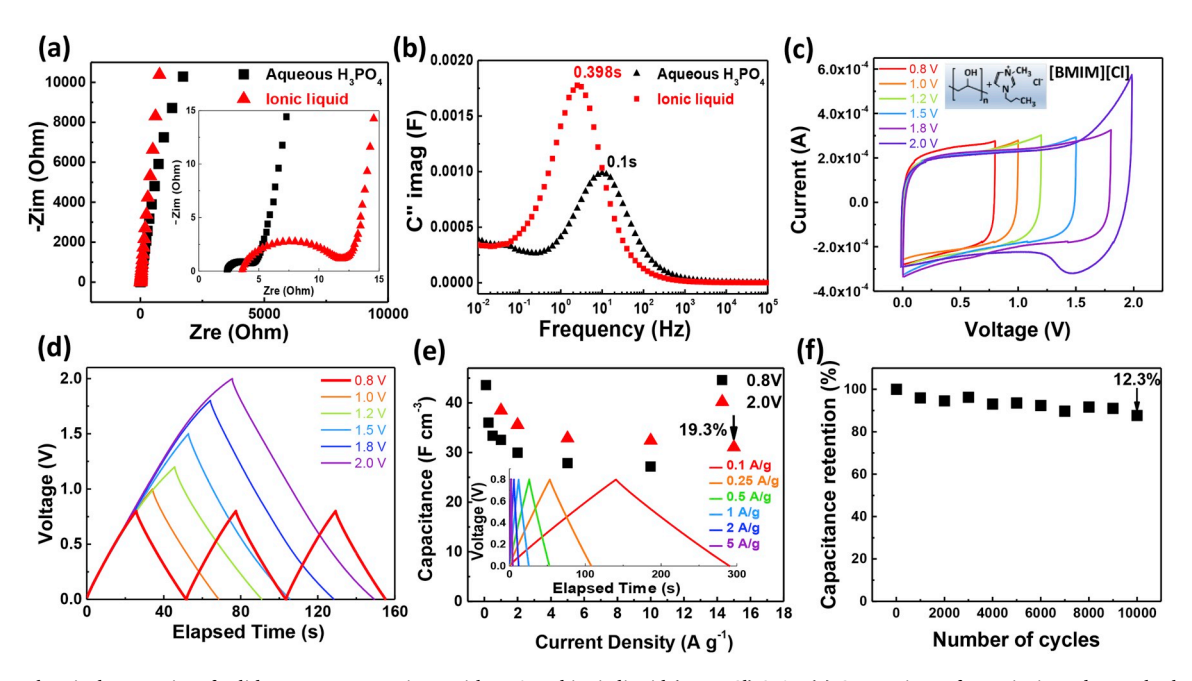


Fig. 3. Electrochemical properties of solid-state supercapacitors with PVA and ionic liquid (BMIMCl) 85%. (a) Comparison of Nyquist impedance plot between ionic liquid and  $H_3PO_4$ . (b) Relaxation time for the aqueous and ionic liquid-based electrolyte system, which is calculated from the imaginary part and frequency. (c) Cyclic voltammetry curves of ionic liquid-based device at 50 mV s<sup>-1</sup> with various voltage: 0.8, 1.0, 1.1, 1.2, 1.6, 1.8, and 2.0 V. (d) Comparison of Galvano static charge/discharge curves of the ionic liquid-based device between 0.8 V and 2 V at current density 1 A g<sup>-1</sup>. (e) Specific capacitances of the ionic liquid-based device at various current densities. Inset is Galvano static charge/discharge curves at different current density. (f) Cyclic stability of ionic liquid-based device at 0–2 V of voltage window.

# 3.2. Characterizations of the supercapacitors in $H_3PO_4$ based electrolyte system

Fig. 2 presents various electrochemical properties of the symmetric solid-state supercapacitor: metal layer/VA-SWNT/PVA (H<sub>3</sub>PO<sub>4</sub> aqueous solution integrated membrane) || PVA (H<sub>3</sub>PO<sub>4</sub> aqueous solution integrated membrane)/VA-SWNT/metal layer. To characterize the evolution of the kinetic parameters, the electrochemical impedance spectroscopy (EIS) was performed by applying a sine wave of 10 mV amplitude over a frequency range from 1 MHz to 1 mHz (Fig. 2a). EIS graphs (Nyquist plots) show one depressed semicircle in the high and intermediate frequency region, which generally correspond to the charge transfer through the electrode/electrolyte interface. The Nyquist plot shows that the electrolyte resistance of the integrated supercapacitors with  $H_3PO_4$  electrolyte is about 2.2  $\Omega$  and the charge-transfer resistance is about  $1.86 \,\Omega$ . This result suggests the fast charge transfer process in the integrated device. At low frequencies, the capacitor manifests its real capacity of charge accumulation and the line close to 90° indicates the effective capacitance of the device.

Cyclic voltammetry was performed at different voltage scan rates from 10 mV s<sup>-1</sup> to 500 mV s<sup>-1</sup> (Fig. 2b). The most of rectangular CV curves are known to exhibit the ideal capacitive behavior of the supercapacitor, indicating that the stored charge is due to an electrochemical double layer. The box-like shape of CV curves remains undistorted even at high rates such as 500 mV s<sup>-1</sup>, implying low contact resistances in the devices as observed in Fig. 2a. The galvanostatic charge/discharge curves also present symmetric and triangular shape in the total range of voltage (0-0.8 V for aqueous electrolyte and 0-2 V for ionic liquid electrolyte) in all applied current densities, implying the reversible capacitive performance (inset figure in Fig. 2c) with the coulombic efficiency ranging from 88% at  $0.1\,\mathrm{A\,g^{-1}}$  to 100% at 20  $\mathrm{A\,g^{-1}}$ . Fig. 2a shows 1) the electrical resistances of electrodes, 2) the ions diffusion resistance, and 3) the interfacial resistance between the electrode and electrolyte. These are consistent with the internal resistance derived using the voltage drop shown in Fig. 2d. The calculated capacitance from the discharge curve of one electrode is  $28.4\,\mathrm{F\,cm}^{-3}$  at a current density of  $0.1\,\mathrm{A\,g}^{-1}$ . The device maintains up to 86% of its capacitance with increasing current densities  $% \left( 1\right) =\left( 1\right) \left( 1\right) \left$ from 0.1 A g<sup>-1</sup> to 20 A g<sup>-1</sup> showing a good rate capability (insert in Fig. 2c). The cyclic stability of the integrated device with H<sub>3</sub>PO<sub>4</sub> based electrolyte system was evaluated using the galvanostatic charge-discharge technique conducted at 1.0 A g $^{-1}$  (Fig. 2d). The device shows close to 100% coulombic efficiency even after 10,000 cycles with no considerable capacitance loss, revealing its outstanding electrochemical stability. Those results could be due to the efficient integration of electrolyte and electrode that also assures the proper electrode/electrolyte interface ensuring the good access to the ions at the high surface area of the VA-SWNTs with the effective double-layer formation.

# 3.3. Characterizations of the supercapacitors in ionic liquid-based electrolyte system

In order to demonstrate an ability to reconfigure electrolyte system for higher power applications, the highly porous VA-SWNTs/PVA film was filled with BMIMCl (containing 15% DI water) instead of  $\rm H_3PO_4$  and operated at higher voltages. The new symmetrical cell was fabricated as the following configuration: metal layer/VA-SWNT/PVA (85 wt% BMIMCl solution integrated membrane) | PVA (85 wt% BMIMCl solution integrated membrane) | PVA (85 wt% BMIMCl solution integrated membrane)/VA-SWNT/metal layer. In Fig. 3a, EIS was used to characterize the resistance. Two different integrated supercapacitors with the aqueous acid and ionic liquid electrolytes are shown. In the low-frequency region, both impedance plots increase sharply and tend to become vertical lines, which are the characteristics of capacitive behaviors of supercapacitors [54]. At the high to medium frequencies, the Nyquist plot clearly shows a semicircle, which represents a low equivalent series resistance (ESR) relying on the contribution of the efficient electrode and electrolyte interface [55].

The electrolyte resistance of the supercapacitor in the ionic liquid-based electrolyte system is about  $3.63\,\Omega$  and the charge-transfer resistance is about  $6.24\,\Omega,$  which is a slightly larger value compared to the  $H_3PO_4$  based electrolyte system, but it still shows a sufficiently small value for resistance.

The maximum phase angle of the ionic liquid-based supercapacitor is about  $-85^{\circ}$ , close to  $-90^{\circ}$  for an ideal capacitor (Fig. S4). For the relaxation time of the supercapacitor, the real (C') and imaginary (C") parts of capacitance change with respect to frequency are shown in Fig. 3b and supplement Fig. S5. The low frequency value of C' is characteristic of the electrode structure and the electrode/electrolyte interface. In contrast, C" corresponds to energy dissipation by an irreversible process. Consequently, the integrated supercapacitors oscillate between two states such as resistance at high frequency and capacitance at low frequency. The relaxation time constant,  $\tau_0$  can be calculated by the equation  $\tau_0 = 1/f_0$ . This time constant corresponds to the value of  $+45^{\circ}$ for the phase angle  $\phi$ . It represents a transition for the supercapacitor between a resistive behavior for a frequency higher than  $1/\tau_0$  and a capacitive behavior for frequency lower than  $1/\tau_0$ . The time constant  $\tau_0$  was found to be about 0.100s for the aqueous based supercapacitor and 0.398s for the ionic liquid-based supercapacitor (Fig. 3b), which is even lower than 10s for the activated carbon supercapacitor [54] and 0.680s for the all solid-state supercapacitor [56]. This result may indicate the relatively low capacitance of the electrode material but also indicate a fast charge transfer due to the favorable interface of the electrode and the electrolyte in the integration supercapacitor [57].

A stable potential window for the ionic liquid-based supercapacitor was observed by cyclic voltammetry (Fig. 3c) and charge/discharge measurements (Fig. 3d) in the range from 0.8 to 2.0 V. The supercapacitor device based on the ionic liquid containing 15% water was stable up to 2.0 V, as shown in Fig. 3c. We note that the CV curves became asymmetric with a sharp current increase/decrease near 2 V. This phenomenon might be the result of chemical reaction/decomposition when the voltage was increased beyond 2.0 V (see supplementary materials, Figs. S6 and S7). Hence, a maximum cell voltage up to 2.0 V was used to evaluate the device performance. The galvanostatic charge/ discharge curves in Fig. 3d show symmetric and triangular shapes for both 0.8 V and 2.0 V. High capacitance values could be obtained for the ionic liquid-based supercapacitors: 32.6 F cm-3 and 38.5 F cm-3 for the devices operating at 0.8 V and 2.0 V, respectively at the current density of 1.0 A g<sup>-1</sup> and calculated from the discharge curve considering the mass of one electrode. In addition, our device could be operated in a stable voltage window of 2.0 V even at a high current density of 15 A g<sup>-1</sup> (Fig. 3e). The coulombic efficiency ranges from 86% at  $1 \text{ A g}^{-1}$  to 100% at 15 A g<sup>-1</sup>. The device operating at 2.0 V presents a good rate capability keeping around 81% of the capacitance from  $1\,\mathrm{A\,g}^{-1}$  to  $15\,\mathrm{A\,g}^{-1}$ . The cycling stability of the ionic liquid-based supercapacitor device was tested at a constant current density of  $1\,\mathrm{Ag}^{-1}$  for 10,000 cycles. As shown in Figs. 3f and 88% of the initial capacitance was retained, indicating good long-term stability. Those characteristics are due to the factors such as the appropriate electrode/electrolyte interface ensuring good wettability, and ion accessibility to transfer large amounts of charge to individual surfaces of high-density VA-SWNT electrodes.

Furthermore, the electrochemical performance of this ionic liquid-based reconfigurable device was tested by mechanically bending up to  $170^\circ$  (Fig. S8) for their possible applications in wearable electronic devices. We observed that the capacitance (calculated from cyclic voltammetry) increased with increasing bending angle. A  $170^\circ$  bent device shows  $45.7~\mathrm{F~cm}^{-3}$  of capacitance that is 19% higher than the capacitance of the flat supercapacitor. This is presumably because the interdistance of two electrodes becomes closer by the mechanical pressure.

#### 3.4. Power and energy densities

The galvanostatic charge/discharge curves were used to evaluate the power and energy density of the integrated flexible supercapacitors. As

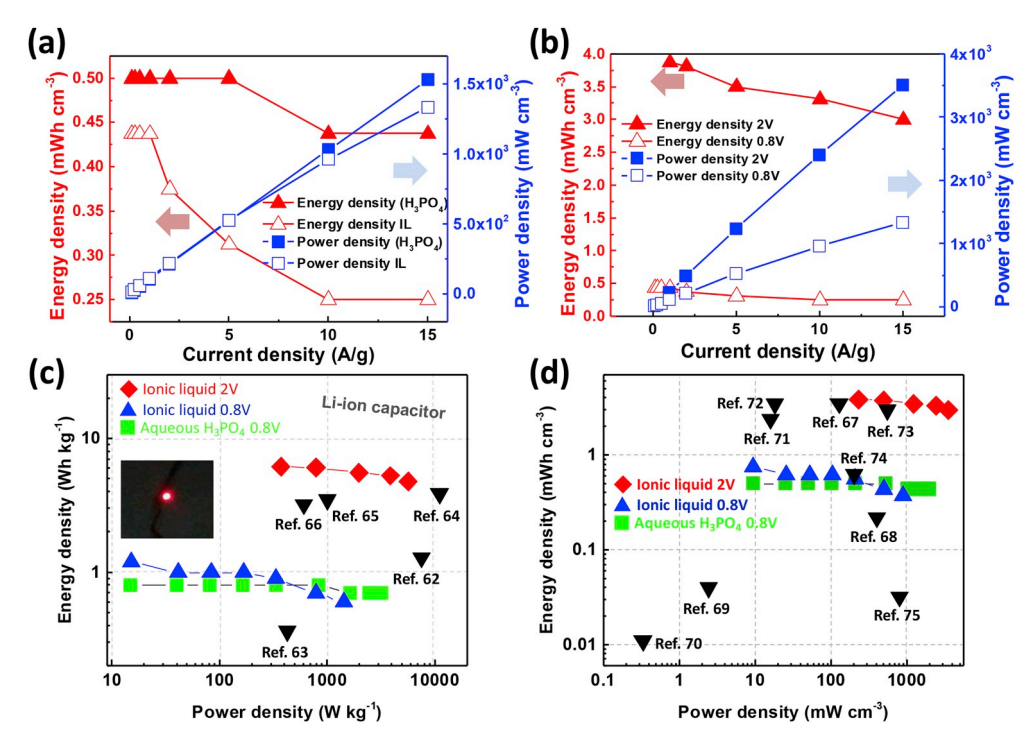


Fig. 4. Energy and power densities of supercapacitor devices. (a, b) Energy density and power density changes along with the current density changes: (a) Comparison of ionic liquid and  $H_3PO_4$  at 0.8 V. (b) Comparison of ionic liquid at 0.8 V and 2 V. (c) Weight-based Ragone plot [48,58–60], with references (Ref. [62–65], and [66].) Inset in (c) is the photograph of LED light testing. (d) Volumetric Ragone plot, with references (Ref. [67–74], and [75].).

shown in the Ragone plot [48,58–60] (Fig. 4c and d), there are no considerable differences between the cells prepared with the aqueous and ionic liquid-based electrolytes at the working voltage of 0.8 V (Fig. 4a). However, it is clear that the electrolyte prepared with 85% ionic liquid in our nanoporous matrix of PVA allows the cell to work considerably stable at 2.0 V. The ionic liquid-based supercapacitor operated at 2.0 V showed superior energy and power densities than many carbon-based electrochemical double layer capacitors (EDLCs) described in the literature [1,36–46,61].

We compare the power and energy density of the ionic liquid-based supercapacitor at 0.8 V and 2.0 V with increasing current densities from  $0.1 \,\mathrm{A\,g^{-1}}$  to  $15\,\mathrm{A\,g^{-1}}$  (Fig. 4b). As expected both the power and the energy densities calculated from the 2.0 V measurements showed much higher values. For the ionic liquid-based supercapacitor, the maximum power density is 3510 mW cm<sup>-3</sup> and the maximum energy density is  $3.875 \,\mathrm{mWh}\,\mathrm{cm}^{-3}$  at  $2.0 \,\mathrm{V}$  operation. The energy and the power densities at the current density of 15 A g<sup>-1</sup> increased 12 and 2.5 times over the value calculated at 0.8 V, respectively. In Fig. 4c and d, the weight based and volumetric energy and power densities of our devices are compared to those of conventional energy storage devices (Please see Fig. S9 for the weight-based capacitances and Fig. S10 for areal-based Ragone plot). The ionic liquid-based supercapacitor is superior to the EDLC devices [63-78] and has excellent performance close to the Li-ion supercapacitor [79,80]. For demonstrating the practical potential of the integrated supercapacitors, the ionic liquid electrolyte based device was used to light up a red light-emitting-diode (LED) (insert figure in Fig. 4c and supplement Fig. S11). LED was successfully turned on for 7 min after being charged for 20 min at 2.2 V.

#### 4. Conclusions

In summary, we design and build all-solid-state and reconfigurable supercapacitors by integrating PVA based solvent exchangeable membranes and super-flat VA-SWNTs. The unique porous PVA membrane structures provide a universal platform where aqueous, organic and ionic liquid-based electrolyte can be selectively used to modulate the

supercapacitor performance even under severe mechanical deformation regardless of the used electrode. The resulting ionic liquid electrolyte-based supercapacitor exhibits stable operation at voltage window 0–2 V and excellent long-term stability and yields high capacitance, energy, and power performance.

## **Author contributions**

These authors (SH and HK) contributed equally to this work. SH, HK and RLL are involved in the development of the idea, preparation of the materials and devices, physical and electrochemical characterization and discussions of the results. HYJ, SG and YJJ are involved in the development of the idea, discussions of the results and coordination of the research group.

#### Notes

Conflicts of interest: There are no conflicts to declare.

#### Acknowledgement

This research was supported by National Science Foundation-DMEREF (1434824) and PFI (1701043) grants and Technology Innovation Program (10050481) funded by the Ministry of Trade, Industry & Energy of Republic of Korea. HYJ acknowledges the National Research Foundation of Korea (NRF) funded by the Ministry of Science and ICT (NRF-2015R1C1A1A01053890, 2017R1A4A1015711). RLL thanks to the Federal University of Minas Gerais - UFMG/Brazil for the license granted for the sabbatical period at the Northeastern University.

### Appendix A. Supplementary data

Supplementary data to this article can be found online at https://doi.org/10.1016/j.jpowsour.2019.05.065.

#### References

- [1] M.G. Hahm, A.L.M. Reddy, D.P. Cole, M. Rivera, J.A. Vento, J. Nam, H.Y. Jung, Y. L. Kim, N.T. Narayanan, D.P. Hashim, C. Galande, Y.J. Jung, M. Bundy, S. Karna, P. M. Ajayan, R. Vajtai, Carbon nanotube-nanocup hybrid structures for high power supercapacitor applications, Nano Lett. 12 (11) (2012) 5616–5621.
- [2] M. Koo, K.I. Park, S.H. Lee, M. Suh, D.Y. Jeon, J.W. Choi, K. Kang, K.J. Lee, Bendable inorganic thin-film battery for fully flexible electronic systems, Nano Lett. 12 (9) (2012) 4810–4816.
- [3] Y. Meng, Y. Zhao, C. Hu, H. Cheng, Y. Hu, Z. Zhang, G. Shi, L. Qu, All-graphene core-sheath microfibers for all-solid-state, stretchable fibriform supercapacitors and wearable electronic textiles, Adv. Mater. 25 (16) (2013) 2326–2331.
- [4] M. Kim, C. Lee, J. Jang, Fabrication of highly flexible, scalable, and high-performance supercapacitors using polyaniline/reduced graphene oxide film with enhanced electrical conductivity and crystallinity, Adv. Funct. Mater. 24 (17) (2014) 2489–2499.
- [5] X. Li, T. Zhao, Q. Chen, P. Li, K. Wang, M. Zhong, J. Wei, D. Wu, B. Wei, H. Zhu, Flexible all solid-state supercapacitors based on chemical vapor deposition derived graphene fibers, Phys. Chem. Chem. Phys. 15 (41) (2013) 17752–17757.
- [6] G. Xiong, C. Meng, R.G. Reifenberger, P.P. Irazoqui, T.S. Fisher, Graphitic petal electrodes for all-solid-state flexible supercapacitors, Adv. Energy Mater. 4 (3) (2014).
- [7] X. Zang, Q. Chen, P. Li, Y. He, X. Li, M. Zhu, X. Li, K. Wang, M. Zhong, D. Wu, H. Zhu, Highly flexible and adaptable, all-solid-state supercapacitors based on graphene woven-fabric film electrodes. Small 10 (13) (2014) 2583–2588.
- [8] C. Huang, J. Zhang, N.P. Young, H.J. Snaith, P.S. Grant, Solid-state supercapacitors with rationally designed heterogeneous electrodes fabricated by large area spray processing for wearable energy storage applications, Sci. Rep. 6 (2016) 25684.
- [9] X. Lu, M. Yu, G. Wang, Y. Tong, Y. Li, Flexible solid-state supercapacitors: design fabrication and applications, Energy Environ. Sci. 7 (7) (2014).
- [10] P. Yang, W. Mai, Flexible solid-state electrochemical supercapacitors, Nanomater. Energy 8 (2014) 274–290.
- [11] Z.S. Wu, A. Winter, L. Chen, Y. Sun, A. Turchanin, X. Feng, K. Mullen, Three-dimensional nitrogen and boron co-doped graphene for high-performance all-solid-state supercapacitors, Adv. Mater. 24 (37) (2012) 5130–5135.
- [12] G. Ma, J. Li, K. Sun, H. Peng, J. Mu, Z. Lei, High performance solid-state supercapacitor with PVA–KOH–K3[Fe(CN)6] gel polymer as electrolyte and separator, J. Power Sources 256 (2014) 281–287.
- [13] H. Yu, J. Wu, L. Fan, K. Xu, X. Zhong, Y. Lin, J. Lin, Improvement of the performance for quasi-solid-state supercapacitor by using PVA–KOH–KI polymer gel electrolyte, Electrochim. Acta 56 (20) (2011) 6881–6886.
- [14] C. Meng, C. Liu, L. Chen, C. Hu, S. Fan, Highly flexible and all-solid-state paperlike polymer supercapacitors, Nano Lett. 10 (10) (2010) 4025–4031.
- [15] Q. Chen, X. Li, X. Zang, Y. Cao, Y. He, P. Li, K. Wang, J. Wei, D. Wu, H. Zhu, Effect of different gel electrolytes on graphene-based solid-state supercapacitors, RSC Adv. 4 (68) (2014) 36253–36256.
- [16] C. Huang, P.S. Grant, One-step spray processing of high power all-solid-state supercapacitors, Sci. Rep. 3 (2013) 2393.
- [17] G.P. Pandey, T. Liu, C. Hancock, Y. Li, X.S. Sun, J. Li, Thermostable gel polymer electrolyte based on succinonitrile and ionic liquid for high-performance solid-state supercapacitors, J. Power Sources 328 (2016) 510–519.
- [18] B. Karaman, A. Bozkurt, Enhanced performance of supercapacitor based on boric acid doped PVA-H2SO4 gel polymer electrolyte system, Int. J. Hydrogen Energy 43 (12) (2018) 6229–6237.
- [19] E.J. Lee, K.H. Park, Y.H. Lee, K.G. Kim, Y.U. Jeong, S.Y. Kim, H.D. Kim, Poly (urethane acrylate)-based gel polymer films for mechanically stable, transparent, and highly conductive polymer electrolyte applications, J. Appl. Polym. Sci. 134 (26) (2017).
- [20] N. Li, T. Lv, Y. Yao, H. Li, K. Liu, T. Chen, Compact graphene/MoS 2 composite films for highly flexible and stretchable all-solid-state supercapacitors, J. Mater. Chem. 5 (7) (2017) 3267–3273.
- [21] S. Peng, L. Fan, C. Wei, X. Liu, H. Zhang, W. Xu, J. Xu, Flexible polypyrrole/copper sulfide/bacterial cellulose nanofibrous composite membranes as supercapacitor electrodes, Carbohydr. Polym. 157 (2017) 344–352.
- [22] M. Suleman, M.A.R. Othman, S.A. Hashmi, Y. Kumar, M. Deraman, R. Omar, M.R. M. Jasni, Activated graphene oxide/reduced graphene oxide electrodes and low viscous sulfonium cation based ionic liquid incorporated flexible gel polymer electrolyte for high rate supercapacitors, J. Alloy. Comp. 695 (2017) 3376–3392.
- [23] W. Ma, S. Chen, S. Yang, W. Chen, W. Weng, Y. Cheng, M. Zhu, Flexible all-solid-state asymmetric supercapacitor based on transition metal oxide nanorods/reduced graphene oxide hybrid fibers with high energy density, Carbon 113 (2017) 151-158
- [24] X. Zhang, M. Kar, T.C. Mendes, Y. Wu, D.R. MacFarlane, Supported ionic liquid gel membrane electrolytes for flexible supercapacitors, Adv. Energy Mater. (2018) 1702702
- [25] T. Chen, L. Dai, Carbon nanomaterials for high-performance supercapacitors, Mater. Today 16 (7–8) (2013) 272–280.
- [26] E.H. Kil, K.H. Choi, H.J. Ha, S. Xu, J.A. Rogers, M.R. Kim, Y.G. Lee, K.M. Kim, K. Y. Cho, S.Y. Lee, Imprintable, bendable, and shape-conformable polymer electrolytes for versatile-shaped lithium-ion batteries, Adv. Mater. 25 (10) (2013) 1395–1400.
- [27] S.Y. Lee, W.H. Meyer, G. Wegner, Phase behavior of gel-type polymer electrolytes and its influence on electrochemical properties, ChemPhysChem 6 (1) (2005) 40,53
- [28] J. Hassoun, S. Panero, P. Reale, B. Scrosati, A new, safe, high-rate and high-energy polymer lithium-ion battery, Adv. Mater. 21 (47) (2009) 4807–4810.

- [29] C.M. Hassan, N.A. Peppas, Structure and morphology of freeze/thawed PVA hydrogels, Macromolecules 33 (2000) 2472–2479.
- [30] J.L. Holloway, K.L. Spiller, A.M. Lowman, G.R. Palmese, Analysis of the in vitro swelling behavior of poly(vinyl alcohol) hydrogels in osmotic pressure solution for soft tissue replacement, Acta Biomater. 7 (6) (2011) 2477–2482.
- [31] R. Ricciardi, F. Auriemma, C. De Rosa, Structure and properties of poly(vinyl alcohol) hydrogels obtained by freeze/thaw techniques, Macromol. Symp. 222 (1) (2005) 49–64.
- [32] R. Ricciardi, F. Auriemma, C. Gaillet, C.D. Rosa, F.o. Laupretre, Investigation of the crystallinity of freeze/thaw poly(vinyl alcohol) hydrogels by different techniques, Macromolecular 37 (2004) 9510–9516.
- [33] V.I. Lozinsky, L.G. Damshkaln, I.N. Kurochkin, I.I. Kurochkin, Study of cryostructuring of polymer systems: 28. Physicochemical properties and morphology of poly(vinyl alcohol) cryogels formed by multiple freezing-thawing, Colloid J. 70 (2) (2011) 189–198.
- [34] T. Hatakeyema, J. Uno, C. Yamada, A. Kishi, H. Hatakeyama, Gel-sol transition of poly(vinyl alcohol) hydrogels formed by freezing and thawing, Thermochim. Acta 431 (1–2) (2005) 144–148.
- [35] X. Liu, T. Osaka, All-solid-state electric double-layer capacitor with isotropic high-density graphite electrode and polyethylene oxide/LiClO4 polymer electrolyte, J. Electrochem. Soc. 143 (12) (1996) 3982–3986.
- [36] M.A. Azam, A. Fujiwara, T. Shimoda, Significant capacitance performance of vertically aligned single-walled carbon nanotube supercapacitor by varying potassium hydroxide concentration, Int. J. Electrochem. Sci. 8 (2013) 3902–3911.
- [37] C. Niu, E.K. Sichel, R. Hoch, D. Moy, H. Tennent, High power electrochemical capacitors based on carbon nanotube electrodes, Appl. Phys. Lett. 70 (11) (1997) 1480–1482.
- [38] K.H. An, K.K. Jeon, J.K. Heo, S.C. Lim, D.J. Bae, Y.H. Lee, High-capacitance supercapacitor using a nanocomposite electrode of single-walled carbon nanotube and polypyrrole, J. Electrochem. Soc. 149 (8) (2002).
- [39] J.N. Barisci, G.G. Wallace, R.H. Baughman, Electrochemical characterization of single-walled carbon nanotube electrodes, J. Electrochem. Soc. 147 (12) (2000) 4580–4583.
- [40] R.H. Baughman, A.A. Zakhidov, W.A. De Heer, Carbon nanotubes—the route toward applications, Science 297 (5582) (2002) 787–792.
- [41] J.H. Chen, W.Z. Li, D.Z. Wang, S.X. Yang, J.G. Wen, Z.F. Ren, Electrochemical characterization of carbon nanotubes as electrode in electrochemical double-layer capacitors, Carbon 40 (2002) 1193–1197.
- [42] R.Z. Ma, J. Liang, B.Q. Wei, B. Zhang, C.L. Xu, D.H. Wu, Study of electrochemical capacitors utilizing carbon nanotube electrodes, J. Power Sources 84 (1999) 126–129.
- [43] C. Kim, S. Pyun, H. Shin, Kinetics of double-layer charging/discharging of activated carbon electrodes: role of surface acidic functional groups, J. Electrochem. Soc. 149 (2) (2002).
- [44] S. Shiraishi, H. Kurihara, K. Okabe, D. Hulicova, A. Oya, Electric double layer capacitance of highly pure single-walled carbon nanotubes (HiPcoe Buckytubese) in propylene carbonate electrolytes, Electrochem. Commun. 4 (2002) 593–598.
- [45] S. Shiraishi, H. Kurihara, L. Shi, T. Nakayama, A. Oya, Electric double-layer capacitance of meso/macroporous activated carbon fibers prepared by the blending method, J. Electrochem. Soc. 149 (7) (2002).
- [46] E. Frackowiak, K. Jurewicz, S. Delpeux, F. Béguin, Nanotubular materials for supercapacitors, J. Power Sources 97–98 (2001) 822–825.
- [47] G. Wu, P. Tan, D. Wang, Z. Li, L. Peng, Y. Hu, C. Wang, W. Zhu, S. Chen, W. Chen, High-performance supercapacitors based on electrochemical-induced vertical-aligned carbon nanotubes and polyaniline nanocomposite electrodes, Sci. Rep. 7 (2017) 43676.
- [48] J.L. Holloway, A.M. Lowman, G.R. Palmese, The role of crystallization and phase separation in the formation of physically cross-linked PVA hydrogels, Soft Matter 9 (3) (2013) 826–833.
- [49] S. Hong, T. Lundstrom, R. Ghosh, H. Abdi, J. Hao, S.K. Jeoung, P. Su, J. Suhr, A. Vaziri, N. Jalili, Y.J. Jung, Highly anisotropic adhesive film made from upsidedown, flat, and uniform vertically aligned CNTs, ACS Appl. Mater. Interfaces 8 (49) (2016) 34061–34067.
- [50] S. Roldan, D. Barreda, M. Granda, R. Menendez, R. Santamaria, C. Blanco, An approach to classification and capacitance expressions in electrochemical capacitors technology, Phys. Chem. Chem. Phys. 17 (2) (2015) 1084–1092.
- [51] M.G. Hahm, Y.K. Kwon, A. Busnaina, Y.J. Jung, Structure controlled synthesis of vertically aligned carbon nanotubes using thermal chemical vapor deposition process, J. Heat Transf. 133 (3) (2011).
- [52] H. Abuhimd, G.M. Uddin, A. Zeid, Y.J. Jung, S. Kamarthi, Chemical vapor deposition-grown vertically aligned single-walled carbon nanotubes length assurance, Int. J. Adv. Manuf. Technol. 64 (1–4) (2012) 545–553.
- [53] Y. Homma, Y. Kobayashi, T. Ogino, D. Takagi, R. Ito, Y.J. Jung, P.M. Ajayan, Role of transition metal catalysts in single-walled carbon nanotube growth in chemical vapor deposition, J. Phys. Chem. B 107 (44) (2003) 12161–12164.
- [54] P.L. Taberna, P. Simon, J.F. Fauvarque, Electrochemical characteristics and impedance spectroscopy studies of carbon-carbon supercapacitors, J. Electrochem. Soc. 150 (3) (2003).
- [55] Z. Cao, B.B. Wei, A perspective: carbon nanotube macro-films for energy storage, Energy Environ. Sci. 6 (11) (2013) 3183–3201.
- [56] S.W. Kim, K.N. Kang, J.W. Min, J.H. Jang, Plotter-assisted integration of wearable all-solid-state micro-supercapacitors, Nano Energy 50 (2018) 410–416.
- [57] K. Sheng, Y. Sun, C. Li, W. Yuan, G. Shi, Ultrahigh-rate supercapacitors based on eletrochemically reduced graphene oxide for ac line-filtering, Sci. Rep. 2 (2012) 247.

- [58] P. Simon, Y. Gogotsi, Materials for electrochemical capacitors, Nature materials 7 (11) (2008) 845–854.
- [59] P.J. Hall, M. Mirzaeian, S.I. Fletcher, F.B. Sillars, A.J.R. Rennie, G.O. Shitta-Bey, G. Wilson, A. Cruden, R. Carter, Energy storage in electrochemical capacitors: designing functional materials to improve performance, Energy Environ. Sci. 3 (9) (2010).
- [60] R. Kötz, M. Carlen, Principles and applications of electrochemical capacitors, Electrochim. Acta 45 (2000) 2483–2498.
- [61] Y. Xu, Z. Lin, X. Huang, Y. Liu, Y. Huang, X. Duan, Flexible solid-state supercapacitors based on three-dimensional graphene hydrogel films, ACS Nano 7 (5) (2013) 4042–4049.
- [62] H. Huang, X. Wang, E. Tervoort, G. Zeng, T. Liu, X. Chen, A. Sologubenko, M. Niederberger, Nano-sized structurally disordered metal oxide composite aerogels as high-power anodes in hybrid supercapacitors, ACS Nano 12 (3) (2018) 2753–2763.
- [63] Z. Yang, J. Deng, X. Chen, J. Ren, H. Peng, A highly stretchable, fiber-shaped supercapacitor, Angew. Chem. 125 (50) (2013) 13695–13699.
- [64] Y. Yesi, I. Shown, A. Ganguly, T.T. Ngo, L.C. hen, K.H. Chen, Directly-grown hierarchical carbon nanotube@ polypyrrole core-shell hybrid for highperformance flexible supercapacitors, ChemSusChem 9 (4) (2016) 370–378.
- [65] C. Yu, C. Masarapu, J. Rong, B. Wei, H. Jiang, Stretchable supercapacitors based on buckled single-walled carbon-nanotube macrofilms, Adv. Mater. 21 (47) (2009) 4793–4797.
- [66] L. Zhang, Q. Ding, Y. Huang, H. Gu, Y.E. Miao, T. Liu, Flexible hybrid membranes with Ni (OH) 2 nanoplatelets vertically grown on electrospun carbon nanofibers for high-performance supercapacitors, ACS Appl. Mater. Interfaces 7 (40) (2015) 22669–22677.
- [67] C. Choi, J.A. Lee, A.Y. Choi, Y.T. Kim, X. Lepró, M.D. Lima, R.H. Baughman, S. J. Kim, Flexible supercapacitor made of carbon nanotube yarn with internal pores, Adv. Mater. 26 (13) (2014) 2059–2065.
- [68] X. Xiao, T. Li, P. Yang, Y. Gao, H. Jin, W. Ni, W. Zhan, X. Zhang, Y. Cao, J. Zhong, L. Gong, Fiber-based all-solid-state flexible supercapacitors for self-powered systems, ACS Nano 6 (10) (2012) 9200–9206.
- [69] P. Yang, X. Xiao, Y. Li, Y. Ding, P. Qiang, X. Tan, W. Mai, Z. Lin, W. Wu, T. Li, H. Jin, Hydrogenated ZnO core-shell nanocables for flexible supercapacitors and self-powered systems. ACS Nano 7 (3) (2013) 2617–2626.

- [70] H. Yang, H. Xu, M. Li, L. Zhang, Y. Huang, X. Hu, Assembly of NiO/Ni (OH) 2/ PEDOT nanocomposites on contra wires for fiber-shaped flexible asymmetric supercapacitors, ACS Appl. Mater. Interfaces 8 (3) (2016) 1774–1779.
- [71] B. Wang, X. Fang, H. Sun, S. He, J. Ren, Y. Zhang, H. Peng, Fabricating continuous supercapacitor fibers with high performances by integrating all building materials and steps into one process, Adv. Mater. 27 (47) (2015) 7854–7860.
- [72] L. Kou, T. Huang, B. Zheng, Y. Han, X. Zhao, K. Gopalsamy, H. Sun, C. Gao, Coaxial wet-spun yarn supercapacitors for high-energy density and safe wearable electronics, Nat. Commun. 5 (2014) 3754.
- [73] Y. Luo, Y. Zhang, Y. Zhao, X. Fang, J. Ren, W. Weng, Y. Jiang, H. Sun, B. Wang, X. Cheng, H. Peng, Aligned carbon nanotube/molybdenum disulfide hybrids for effective fibrous supercapacitors and lithium ion batteries, J. Mater. Chem. 3 (34) (2015) 17553–17557.
- [74] Z. Zhang, F. Xiao, S. Wang, Hierarchically structured MnO 2/graphene/carbon fiber and porous graphene hydrogel wrapped copper wire for fiber-based flexible all-solid-state asymmetric supercapacitors, J. Mater. Chem. 3 (21) (2015) 11215–11223.
- [75] C. Zhang, M.P. Kremer, A. Seral Ascaso, S.H. Park, N. McEvoy, B. Anasori, Y. Gogotsi, V. Nicolosi, Stamping of flexible, coplanar micro-supercapacitors using MXene inks, Adv. Funct. Mater. 28 (9) (2018) 1705506.
- [76] P.C. Chen, G. Shen, S. Sukcharoenchoke, C. Zhou, Flexible and transparent supercapacitor based on in 2 O 3 nanowire/carbon nanotube heterogeneous films, Appl. Phys. Lett. 94 (4) (2009), 043113.
- [77] Z. Song, L. Li, D. Zhu, L. Miao, H. Duan, Z. Wang, W. Xiong, Y. Lv, M. Liu, L. Gan, Synergistic design of a N, O co-doped honeycomb carbon electrode and an ionogel electrolyte enabling all-solid-state supercapacitors with an ultrahigh energy density, J. Mater. Chem. 7 (2) (2019) 816–826.
- [78] Z. Song, D. Zhu, L. Li, T. Chen, H. Duan, Z. Wang, Y. Lv, W. Xiong, M. Liu, L. Gan, Ultrahigh energy density of a N, O codoped carbon nanosphere based all-solid-state symmetric supercapacitor, J. Mater. Chem. 7 (3) (2019) 1177–1186.
- [79] V. Aravindan, W. Chuiling, M.V. Reddy, G.S. Rao, B.V. Chowdari, S. Madhavi, Carbon coated nano-LiTi 2 (PO 4) 3 electrodes for non-aqueous hybrid supercapacitors, Phys. Chem. Chem. Phys. 14 (16) (2012) 5808–5814.
- [80] V. Aravindan, Y.L. Cheah, W.F. Mak, G. Wee, B.V. Chowdari, S. Madhavi, Fabrication of high energy-density hybrid supercapacitors using electrospun V2O5 nanofibers with a self-supported carbon nanotube network, ChemPlusChem 77 (7) (2012) 570–575.